

# Wavelet Spectra for Multivariate Point Processes

Edward A. K. Cohen<sup>1</sup> and Alexander J. Gibberd<sup>2</sup>

<sup>1</sup>Department of Mathematics, Imperial College London, South Kensington Campus,  
London SW7 2AZ, U.K.

<sup>2</sup>Department of Mathematics and Statistics, Lancaster University, Bailrigg,  
Lancaster LA1 4YF, U.K.

## Abstract

Wavelets provide the flexibility to detect and analyse unknown non-stationarity in stochastic processes. Here, we apply them to multivariate point processes as a means of characterising correlation structure within and between multiple event data streams. To provide statistical tractability, a temporally smoothed wavelet periodogram is developed for both real- and complex-valued wavelets, and shown to be equivalent to a multi-wavelet periodogram. Under certain regularity assumptions, the wavelet transform of a point process is shown to be asymptotically normal. The temporally smoothed wavelet periodogram is then shown to be asymptotically Wishart distributed with tractable centrality matrix and degrees of freedom computable from the multi-wavelet formulation. Distributional results extend to wavelet coherence; a time-scale measure of inter-process correlation. The presented theory and methodology are verified through simulation and applied to neural spike train data.

## 1 Introduction

We adopt the construction of Hawkes (1971) which presents a  $p$ -dimensional multivariate point process ( $p \geq 1$ ) as a counting vector  $N(t) \equiv (N_1(t), \dots, N_p(t))^T$  where the random element  $N_i(t)$  ( $i = 1, \dots, p$ ) states the number of events of type  $i$  over the interval  $(0, t]$ . Its

first order properties are characterised by its rate  $\lambda(t) \in \mathbb{R}^p$ , defined as  $\lambda(t) \equiv E(dN(t))/dt$  where  $dN(t) = N(t + dt) - N(t)$ , and its second order properties at times  $s$  and  $t$  characterised by its covariance density matrix

$$\Gamma(s, t) = E(dN(s)dN^T(t))/(dt\ ds) - \lambda(s)\lambda^T(t).$$

Process  $N(t)$  is second-order stationary (henceforth referred to simply as “stationary”) if  $\lambda(t)$  is constant for all  $t$  and  $\Gamma(t, s)$  depends only on  $\tau = s - t$ . In this setting we will denote the covariance density matrix  $\Gamma(\tau)$ .

The spectral domain provides a rich environment for representing this second order structure and is based on the fact that stationary stochastic processes can be considered a composite of subprocesses operating at different frequencies. The spectral density matrix of a stationary point process is the Fourier transform of its covariance density matrix (Bartlett, 1963), namely

$$S(f) = \text{diag}(\lambda) + \int_{-\infty}^{\infty} \Gamma(\tau) e^{-i2\pi f\tau} d\tau, \quad -\infty < f < \infty.$$

A fundamental summary of the second order interaction between a pair of component processes,  $N_i(t)$  and  $N_j(t)$  say, is their coherence defined as

$$\rho_{ij}^2(f) = \frac{|S_{ij}(f)|^2}{S_{ii}(f)S_{jj}(f)}. \quad (\text{S1})$$

This provides a normalised measure on  $[0, 1]$  of the correlation structure between the processes in the frequency domain. For time series data, it has been used extensively in several disciplines, including climatology, oceanography and medicine. For event data, it has been an important tool in neuroscience for the analysis of neuron spike train data.

Estimation of the coherence can be achieved by substituting smoothed spectral estimators into (S1). Failure to smooth (i.e. simply using the periodogram) will result in a coherence estimate of one for all frequencies, irrespective of whether correlation exists between the pair of processes or not. Tractability of the coherence estimator’s distribution is crucial for principled statistical testing and dependent on the smoothing procedure used (Walden, 2000).

In reality, stochastic processes do not conform to the strict assumptions of stationarity. This might occur through simple first-order trends in the underlying data generating process, or

more typically, complex changes in the second (or higher) order structure of the process. This renders classical Fourier methods obsolete and demands more flexible non-parametric methodology, with wavelets forming a natural basis with which to analyses non-stationary behaviour at different scales.

For a wavelet  $\psi(t)$ , the continuous wavelet transform at scale  $a > 0$  and translation (or time)  $b \in \mathbb{R}$  of  $N(t)$ , observed on the interval  $(0, T]$ , is defined as (Brillinger, 1996)

$$w(a, b) = a^{-1/2} \int_0^T \psi^* \left( \frac{t-b}{a} \right) dN(t), \quad (\text{S2})$$

where  $*$  denotes complex conjugation. The  $i$ th element of this stochastic integral is computed as  $w_i(a, b) = \sum_{k=1}^{N_i(T)} \psi_{a,b}^*(s_{i,k})$ , where  $s_{i,1}, \dots, s_{i,N_i(T)}$  are the ordered event times of  $N_i(t)$  and  $\psi_{a,b}(t) \equiv a^{-1/2}\psi((t-b)/a)$ . Thus, working with the continuous time process is possible if the finite set of event times are known. The wavelet periodogram is subsequently defined as

$$W(a, b) = w(a, b)w^H(a, b).$$

The diagonal element  $W_{ii}(a, b) = w_i(a, b)w_i^*(a, b)$  ( $i = 1, \dots, p$ ) is the wavelet periodogram for  $N_i(t)$ , and the off-diagonal element  $W_{ij}(a, b) = w_i(a, b)w_j^*(a, b)$  ( $i \neq j$ ) is the cross wavelet periodogram for processes  $N_i(t)$  and  $N_j(t)$ .

As is the case with the Fourier periodogram, smoothing is required for two reasons. First is to control variance, second is to give meaningful values of the wavelet coherence estimator. Wavelet coherence is an analogue of coherence which provides a normalised measure on  $[0, 1]$  of the correlation between a pair of processes in time-scale space. It is defined as

$$\gamma_{ij}^2(a, b) = \frac{|\Omega_{ij}(a, b)|^2}{\Omega_{ii}(a, b)\Omega_{jj}(a, b)}$$

where  $\Omega$  is a smoothed version of  $W$ . In the time series setting, it has again been extensively applied in a wide range of disciplines. Crucial for rigorous statistical analysis and testing is the use of a smoothing method for which distributional results can be derived, as has been achieved in the Gaussian time series setting (Cohen & Walden, 2010a,b).

In this paper we demonstrate that temporal smoothing can be used for continuous time event data to produce a statistically tractable estimator for wavelet spectra and coherence in the multivariate point process setting.

## 2 Temporally smoothed wavelet periodogram

### 2.1 Formulation

Let  $\psi(t)$  be a continuous wavelet and  $h(t)$  a symmetric window function with compact support and normalised such that  $\int_{-\infty}^{\infty} h(t)dt = 1$ . The *temporally smoothed wavelet periodogram (TSWP)* is defined as

$$\Omega(a, b) = \int_{-\infty}^{\infty} h(b' - b)W(a, b')db', \quad (\text{S3})$$

and is analogous to Welch's *weighted overlapping sample averaging (WOSA)* spectral estimator for stationary time series (Welch, 1967; Carter, 1987). It will be convenient to consider smoothing windows whose width scales with  $a$ , we will therefore consider smoothing windows of the form  $h_a(t) = a^{-1}h(t/a)$ . Defining the hermitian kernel function

$$K(s, t) = \int_{-\infty}^{\infty} h(b')\psi(s - b')\psi^*(t - b')db', \quad (\text{S4})$$

the TSWP in (S3) can be expressed as

$$\Omega(a, b) \equiv \int_0^T \int_0^T K_{a,b}(s, t)dN(t)dN^T(s),$$

where  $K_{a,b}(s, t) = a^{-1}K((s - b)/a, (t - b)/a)$ . The  $(i, j)$ th element of  $\Omega(a, b)$  is computed as

$$\Omega_{ij}(a, b) = \sum_{k=1}^{N_i(T)} \sum_{k'=1}^{N_j(T)} K_{a,b}(s_{i,k}, s_{j,k'}),$$

where  $\{s_{i,k}; k = 1, \dots, N_i(T)\}$  and  $\{s_{j,k'}; k' = 1, \dots, N_j(T)\}$  are the event times of processes  $N_i(t)$  and  $N_j(t)$ , respectively ( $i, j = 1, \dots, p$ ).

Given a choice for  $h(t)$ , the form of  $K(s, t)$  will depend on  $\psi(t)$ . Throughout this paper, we use the examples of the complex-valued Morlet wavelet and the real-valued Mexican hat wavelet. These are examples of wavelets for which  $K(s, t)$  is analytically tractable.

## 2.2 Practical implementation

For continuous time wavelet analysis, the wavelets themselves are often non-compactly supported. However, the region of significant support is typically well localized and a close approximation to  $w(a, b)$  can be obtained through utilising the approximating wavelet

$$\bar{\psi}(t) = \begin{cases} \psi(t) & |t| < \alpha/2 \\ 0 & \text{otherwise.} \end{cases}$$

For example, the Morlet wavelet  $\psi(t) = \pi^{-1/4} e^{-t^2/2} e^{i2\pi t}$  shown in Fig. 1 has infinite support but can be well approximated by  $\bar{\psi}(t)$  for  $\alpha = 8$ . In practice, to speed up computation, it can make sense to use the approximating wavelet as only a subset of the data is required to compute the wavelet transform. From herein, to simplify notation, will we use  $\psi(t)$  to represent both the original and approximating wavelet, assuming that  $\alpha$  is chosen correctly.

In a finite data setting we are restricted in what regions of the time-scale space we can fairly evaluate (S2) without the consequences of edge effects at either ends of the data. For the continuous wavelet transform and wavelet periodogram, we restrict ourselves of values of  $a$  and  $b$  that satisfy  $\text{supp}(\bar{\psi}_{a,b}) = (b - a\alpha/2, b + a\alpha/2) \subseteq (0, T]$ . This defines an isosceles triangle  $\mathcal{T}_{\alpha,T} \subset \mathbb{R}^2$  with vertices  $(0, 0)$ ,  $(0, T)$  and  $(a_{\max}, T/2)$  where  $a_{\max} = T/\alpha$ . Its interior contains all valid pairs of  $(a, b)$ , i.e. for some scale  $a \in (0, a_{\max})$ , the wavelet transform is valid for all  $b \in (a\alpha/2, T - a\alpha/2)$ .

When smoothing in time, we have to be more conservative with the ranges of  $a$  and  $b$  we can take. For a smoothing window  $h(t)$  with support  $\text{supp}(h) = (-\kappa/2, \kappa/2)$ , the effective support of  $K(s, t)$  is  $\text{supp}(K) = (-(\alpha + \kappa)/2, (\alpha + \kappa)/2) \times (-(\alpha + \kappa)/2, (\alpha + \kappa)/2)$ , and therefore we restrictive ourselves to values of  $a$  and  $b$  for which  $\text{supp}(K_{a,b}) = (b - a(\alpha + \kappa)/2, b + a(\alpha + \kappa)/2) \times (b - a(\alpha + \kappa)/2, b + a(\alpha + \kappa)/2) \subseteq (0, T] \times (0, T]$ . Again, this defines an isosceles triangle  $\mathcal{T}_{\alpha,\kappa,T} \subset \mathbb{R}^2$ , on this occasion with vertices  $(0, 0)$ ,  $(0, T)$  and  $(a_{\max}, T/2)$ , where  $a_{\max} = T/(\alpha + \kappa)$ . Its interior contains all valid pairs of  $(a, b)$ , i.e., for some scale  $a \in (0, a_{\max})$ , the TSWP is valid for all  $b \in (a'(\alpha + \kappa)/2, T - a'(\alpha + \kappa)/2)$ . In practice, a positive minimum value of  $a$  should be imposed to ensure a reasonable amount of event data exists in the smoothing range.

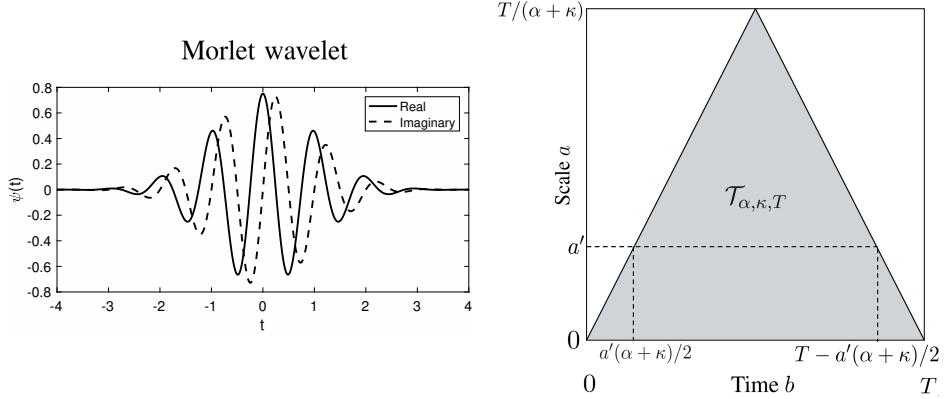


Figure 1: The Morlet wavelet and the valid region for analysis  $\mathcal{T}_{\alpha, \kappa, T}$ . Note this has been plotted with time  $b$  on the horizontal axis and scale  $a$  on the vertical axis, as is convention

### 3 Multi-wavelet representation

#### 3.1 Formulation

Associated with kernel  $K(s, t)$  is the hermitian linear operator  $T_K$  defined as  $[T_K f](t) = \int_{-\infty}^{\infty} K(s, t)f(s)ds$ . Given  $K(s, t)$  is non-negative definite, it follows from Mercer's Theorem (Mercer, 1909) that  $K(s, t) = \sum_{l=0}^{\infty} \eta_l \varphi_l(s) \varphi_l^*(t)$  where  $\{\varphi_l(t); l = 0, 1, \dots\}$  are the orthonormal eigenfunctions of  $T_K$  with non-zero eigenvalues  $\{\eta_l; l = 0, 1, \dots\}$  ordered in decreasing size. Noting that  $\text{tr}(T_K) := \int_{-\infty}^{\infty} K(t, t)dt = 1$ , it follows that  $\sum_{l=0}^{\infty} \eta_l = 1$ . From here on, we refer to  $\{\varphi_l(t); l = 0, 1, \dots\}$  as the eigenfunctions of  $K(s, t)$ . The following proposition shows that these orthonormal eigenfunctions are themselves wavelets. The proof can be found in Supplementary Material Section 1.

**Proposition 1.** *Let  $\psi(t)$  be a wavelet and  $h(t)$  a smoothing window that generates a non-negative definite kernel  $K(s, t)$  with corresponding eigenfunctions  $\{\varphi_l(t); l = 0, 1, \dots\}$ . Every eigenfunction  $\varphi_l(t)$  with non-zero eigenvalue satisfies the conditions of a wavelet, namely: (i)  $\int_{-\infty}^{\infty} \varphi_l(t)dt = 0$ , (ii)  $\|\varphi_l\| = 1$ , (iii) (the admissibility condition)  $\int_{-\infty}^{\infty} f^{-1} |\Phi_l(f)|^2 df < \infty$ , where  $\Phi_l$  is the Fourier transform of  $\varphi_l(t)$ .*

We therefore adopt the term *eigen-wavelets* for the functions  $\{\varphi_l(t); l = 0, 1, \dots\}$ .

Turning our attention back to the TSWP, through a change in variable, it is straightforward to show

$$\int_{-\infty}^{\infty} K_{a,b}(s, t) \varphi_l((t - b)/a) dt = \eta_l \varphi_l((s - b)/a).$$

Thus, the scaled and shifted versions  $\{\varphi_{l,a,b}(t) = a^{-1/2} \varphi_l((t - b)/a); l = 0, 1, \dots\}$  of the eigen-wavelets are themselves the eigenfunctions of  $K_{a,b}$ , and again from Mercer's theorem  $K_{a,b}(s, t) = \sum_{l=0}^{\infty} \eta_l \varphi_{l,a,b}(s) \varphi_{l,a,b}^*(t)$  (Mercer, 1909). The TSWP can therefore be represented as

$$\Omega(a, b) = \sum_{l=0}^{\infty} \eta_l v_l(a, b) v_l^H(a, b) \quad (\text{S5})$$

where  $v_l(a, b) = \int_0^T \varphi_{l,a,b}(t) dN(t)$  is the continuous wavelet transform of  $N(t)$  at scale  $a$  and translation  $b$  with respect to eigen-wavelet  $\varphi_l(t)$ . We therefore note that the TSWP is equivalent to the weighted sum of wavelet spectra arising from the orthonormal eigen-wavelet system. This is analogous to multitapering (Thomson, 1982) and comparisons can also be drawn with the multi-wavelet spectrum of Cohen & Walden (2010b). In that setting, multiple orthogonal wavelets were derived in Olhede & Walden (2002) from a time-frequency concentration problem, whereas here we have shown they can be generated by any arbitrary wavelet  $\psi(t)$  and smoothing window  $h(t)$ .

The representation in (S5) will be crucial for deriving the distributional results in Section 4.1, as well as offering computational speed-up. In general, closed form expressions for the eigen-wavelets  $\{\varphi_l(t); l = 0, 1, \dots\}$  will be unobtainable and numerical procedures need to be used to find the solutions of  $\int_{-\infty}^{\infty} K(s, t) \varphi_l(t) dt = \eta_l \varphi_l(s)$ . Details for an implementation of the Nystrom method for doing just this can be found in Appendix 1.

## 3.2 Worked example

The Morlet wavelet  $\psi(t) = \pi^{-1/4} e^{-t^2/2} e^{i2\pi t}$  can be seen as a complex sinusoid enveloped with a Gaussian window, and therefore the wavelet transform at scale  $a > 0$  and translation  $b$  is the Fourier transform of the tapered process, localised at  $b$  and evaluated at frequency

$1/a$ . The TSWP using a rectangular smoothing window

$$h(t) = \begin{cases} 1/\kappa & -\kappa/2 < t < \kappa/2 \\ 0 & \text{otherwise,} \end{cases}$$

emits kernel

$$K(s, t) = \frac{1}{2\kappa} e^{-(t-s)^2} (\operatorname{erf}(\kappa - (t+s)) + \operatorname{erf}(\kappa + (t+s))) e^{-i2\pi(t-s)}$$

where  $\operatorname{erf}(x) = \pi^{-1/2} \int_{-x}^x \exp(-t^2) dt$  is the Gauss error function. The real part of this kernel is shown in Fig. 2a.

The kernel can be expressed as  $K(s, t) = e^{i2\pi s} k(s, t) e^{-i2\pi t}$  where  $k(s, t) = (2\kappa)^{-1} e^{-(t-s)^2} (\operatorname{erf}(\kappa - (t+s)) + \operatorname{erf}(\kappa + (t+s)))$  is itself a real valued symmetric kernel with its own set of real valued orthonormal eigenfunctions  $\{\phi_l; l = 0, 1, \dots\}$  and associated eigenvalues  $\{\eta_l; l = 0, 1, \dots\}$ . It follows that  $\varphi_l(t) = e^{i2\pi t} \phi_l(t)$  is an eigenfunction of  $K(s, t)$  with corresponding eigenvalue  $\eta_l$  and hence  $\{\varphi_l(t) = e^{i2\pi t} \phi_l(t); l = 0, 1, \dots\}$  is the eigen-wavelet system emitted by the Morlet wavelet with a rectangular smoothing window. The first five of these eigen-wavelets for  $\kappa = 10$  are shown in Fig. 2b. This eigen-wavelet system follows the same spirit of the generating Morlet wavelet, with themselves being complex sinusoids enveloped by a taper. Thus, performing a continuous wavelet transform with one of the eigen-wavelets is equivalent to a time localised tapered Fourier transform evaluated at frequency  $1/a$ , and the TSWP as represented in (S5) is equivalent to a time localised multitaper spectral estimator. As means of a comparison, the kernel and associated eigen-wavelets of the Mexican hat wavelet using a rectangular smoothing window are shown in Fig. 2c and Fig. 2d, respectively.

## 4 Statistical Properties

### 4.1 Preliminaries

The purpose of this paper is to provide methodology for analysing non-stationary processes. However, for theoretically tractable results, statistical analysis will be performed on stationary processes. At first, this may appear contradictory, however, stationarity is

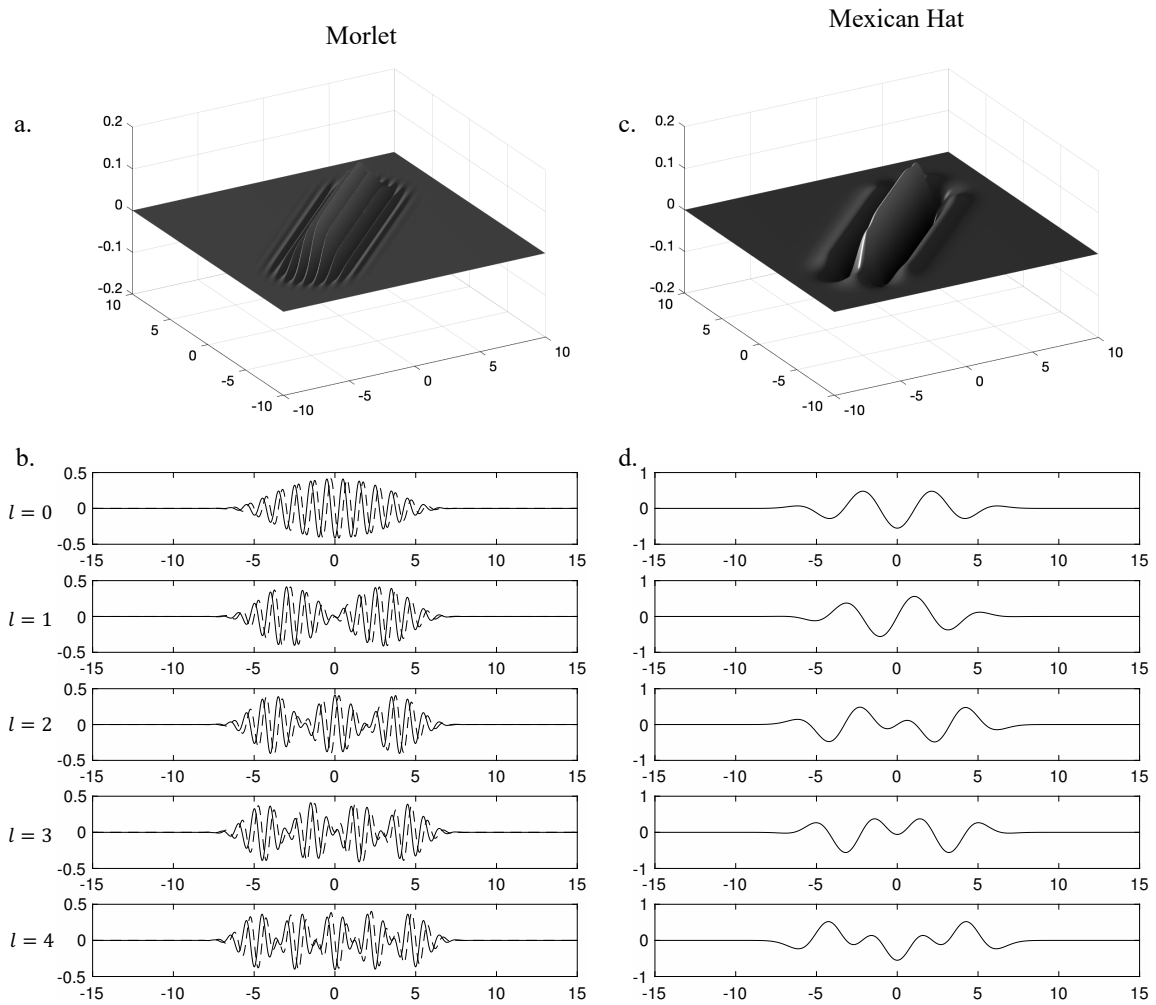


Figure 2: The kernel and first five eigen-wavelets for the Morlet wavelet and Mexican hat wavelet subject to a rectangular smoothing window of width  $\kappa = 10$ .

invariably stipulated as part of any null hypothesis to be tested and is therefore a very natural framework in which to work. Furthermore, point processes with slowly evolving second-order structure may be considered stationary across the support of the wavelet and hence results can readily transfer to the non-stationary setting. Asymptotic results will be shown for  $a$  growing with  $T$ .

Before presenting results on the statistical properties of the TSWP, it becomes necessary to provide the following proposition which shows the effective frequency response of the eigen-wavelet system is equal to the frequency response of the generating wavelet  $\psi(t)$  and does not depend on the choice of smoothing window  $h(t)$ . The proof can be found in Supplementary Material Section 1.

**Proposition 2.** *Let  $\psi(t)$  be a continuous wavelet and  $h(t)$  a smoothing window that generates a non-negative definite kernel  $K(s, t)$  with corresponding eigenfunctions  $\{\varphi_l(t); l = 0, 1, \dots\}$  and eigenvalues  $\{\eta_l; l = 0, 1, \dots\}$ . It holds that  $\sum_l \eta_l |\Phi_l(f)|^2 = |\Psi(f)|^2$  where  $\Phi_l$  and  $\Psi(f)$  are the Fourier transforms of  $\varphi_l(t)$  and  $\psi(t)$ , respectively.*

We also introduce the central frequency of a wavelet (Cohen & Walden, 2010a). For wavelet  $\psi(t)$  with Fourier transform  $\Psi(f)$ , its central frequency is defined as  $f_0 := \int_0^\infty f |\Psi(f)|^2 df$ . The central frequency of  $\psi_{a,b}$  is therefore  $f_0/a$  and can be interpreted as the central analysing frequency of the wavelet at scale  $a$ . For example the Morlet wavelet has a central frequency of  $f_0 = 1$  and the Mexican hat wavelet has a central frequency of (approx.)  $f_0 = 0.21$ . It immediately follows from Proposition 2 that the central frequency of the eigen-wavelet system is  $f_0$ .

**Proposition 3.** *Let  $N(t)$  be a  $p$ -dimensional stationary process with continuous and differentiable spectral density matrix  $S(f)$ , let  $\psi(t)$  be a continuous wavelet with approximating support  $(-\alpha/2, \alpha/2)$ , and let  $h(t)$  be a positive smoothing window, continuous and compactly supported on  $(-\kappa/2, \kappa/2)$ . For all  $(a, b) \in T_{\alpha, \kappa, T}$ ,*

$$E(\Omega(a, b)) = E(W(a, b)) = \int_{-\infty}^{\infty} |\Psi(af)|^2 S(f) df.$$

*Furthermore, if  $a = \epsilon T/(\alpha + \kappa)$ ,  $0 < \epsilon < 1$ , such that  $(a, b) \in \mathcal{T}_{\alpha, T}$ , then as  $T \rightarrow \infty$ ,  $E(\Omega(a, b)) = E(W(a, b)) = S(f_0/a) + O(\tilde{\epsilon}^{-2} T^{-2})$ , where  $\tilde{\epsilon} = \epsilon/(\alpha + \kappa)$ .*

The proof can be found in Supplementary Material Section 1.

The following mixing condition presented as Assumption 2.2 in Brillinger (1972) is sufficient for the asymptotic results that follow. It ensures that dependency structure in the point process decays at a sufficient rate for central limit arguments to be invoked. To do so, we define the  $k$ th order cumulant  $q$  of the differential process as

$$q_{i_1, \dots, i_k}(t_1, \dots, t_k) dt_1 \cdots dt_k \equiv \text{cum}\{\text{d}N_{i_1}(u_1), \dots, \text{d}N_{i_k}(u_k)\}.$$

**Assumption 1.** *The  $p$ -dimensional point process  $N(t)$  is strictly stationary, i.e.  $q_{i_1, \dots, i_k}(t_1 + t, \dots, t_k + t) = q_{i_1, \dots, i_k}(t_1, \dots, t_k)$ , and we set  $r_{i_1, \dots, i_k}(u_1, \dots, u_{k-1}) = q_{i_1, \dots, i_k}(u_1, \dots, u_{k-1}, 0)$ . Furthermore, all moments exist, the cumulant function satisfies*

$$\int_{-\infty}^{\infty} \cdots \int_{-\infty}^{\infty} |r_{i_1, \dots, i_k}(u_1, \dots, u_{k-1})| du_1 \cdots du_{k-1} < \infty,$$

for  $i_1, \dots, i_k = 1, \dots, p$  and  $k = 2, 3, \dots$ , and

$$\int_{-\infty}^{\infty} |u| |r_{i_1, i_2}(u)| du < \infty$$

for  $i_1, i_2 = 1, \dots, p$ .

The following assumption is placed on the smoothing window.

**Assumption 2.** *The smoothing window  $h(t)$  is positive, compactly supported and continuous on  $(-\kappa/2, \kappa/2)$ , integrates to one, and there exists a finite  $C$  such that  $\int |h(t+u) - h(t)| dt < C|u|$ .*

We will proceed with the derivation of the asymptotic distribution for the TSWP in the setting of  $a$  growing with  $T$ . The distributional results differ slightly depending on whether a real-valued wavelet (e.g. Mexican hat) or complex-valued wavelet (e.g. Morlet) is chosen.

## 4.2 Asymptotic distributional results for real-valued wavelets

**Assumption 3.** *The analysing wavelet  $\psi(t)$  is real-valued, continuous, has approximating support  $(-\alpha/2, \alpha/2)$  for some finite  $\alpha$ , and there exists a finite  $C$  such that  $\int |\psi(t+u) - \psi(t)| dt < C|u|$  for all real  $u$ .*

**Theorem 1.** Let  $N(t)$  be a  $p$ -dimensional stationary process satisfying Assumption 1 and with spectral density matrix  $S(f)$ . Let  $\psi(t)$  be a wavelet satisfying Assumption 3 with central frequency  $f_0$ . If  $a = \epsilon T/\alpha$ ,  $0 < \epsilon < 1$ , such that  $(a, b) \in \mathcal{T}_{\alpha, T}$ , then as  $T \rightarrow \infty$ , the continuous wavelet transform  $w(a, b)$  is asymptotically  $\mathcal{N}_p(0, S(f_0/a))$  for all  $b \in (a\alpha/2, T - a\alpha/2)$ .

The proof of this result is built on the work of Brillinger (1972) and is outlined in Supplementary Material Section 1.

Let  $\mathcal{W}_p(n, \Sigma)$  denote the  $p$ -dimensional Wishart distribution with  $n$  degrees of freedom and centrality matrix  $\Sigma$ .

**Theorem 2.** Let  $N(t)$  be a  $p$ -dimensional stationary process satisfying Assumption 1 with spectral density matrix  $S(f)$ . Let  $h(t)$  be a smoothing window satisfying Assumption 2, let  $\psi(t)$  be a wavelet with central frequency  $f_0$  satisfying Assumption 3, and let  $\{\eta_l; l = 0, 1, \}$  be the eigenvalues of the kernel  $K(s, t)$  defined in (S4). If  $a = \epsilon T/(\alpha + \kappa)$ ,  $0 < \epsilon < 1$ , such that  $(a, b) \in \mathcal{T}_{\alpha, \kappa, T}$ , then as  $T \rightarrow \infty$ , the temporally smoothed wavelet periodogram  $\Omega(a, b)$  is asymptotically  $(1/n)\mathcal{W}_p(n, S(f_0/a))$  for all  $b \in (a(\alpha + \kappa)/2, T - a(\alpha + \kappa)/2)$ , where  $n = 1/(\sum_{l=1}^{\infty} \eta_l^2)$ .

The proof of Theorem 2 can be found in Supplementary Material Section 1. We can now state the following corollary for the distribution of the wavelet coherence. We let  ${}_2F_1(\alpha_1, \alpha_2; \beta_1; z)$  denote the hypergeometric function with 2 and 1 parameters  $\alpha_1$ ,  $\alpha_2$  and  $\beta_1$  and scalar argument  $z$ .

**Corollary 1.** Under the conditions of Theorem 2, the temporally smoothed wavelet coherence  $\gamma_{ij}^2(a, b) = |\Omega_{ij}(a, b)|^2/(\Omega_{ii}(a, b)\Omega_{jj}(a, b))$  between component processes  $N_i(t)$  and  $N_j(t)$  ( $i \neq j$ ) asymptotically has density function

$$g_{\gamma^2}(x) = \frac{\Gamma(\frac{1}{2}n)}{\Gamma(\frac{1}{2})\Gamma(\frac{1}{2}(n-1))} x^{-1/2} (1-x)^{(n-3)/2} (1-\rho^2)^{n/2} {}_2F_1(n/2, n/2, 1/2, \rho^2 x)$$

where  $\rho^2$  is shorthand for  $\rho_{ij}^2(f_0/a)$ , the spectral coherence between  $N_i(t)$  and  $N_j(t)$  at frequency  $f_0/a$ . In the null case of  $\rho_{ij}^2(f_0/a) = 0$ , this distribution is Beta( $1/2, (n-1)/2$ ).

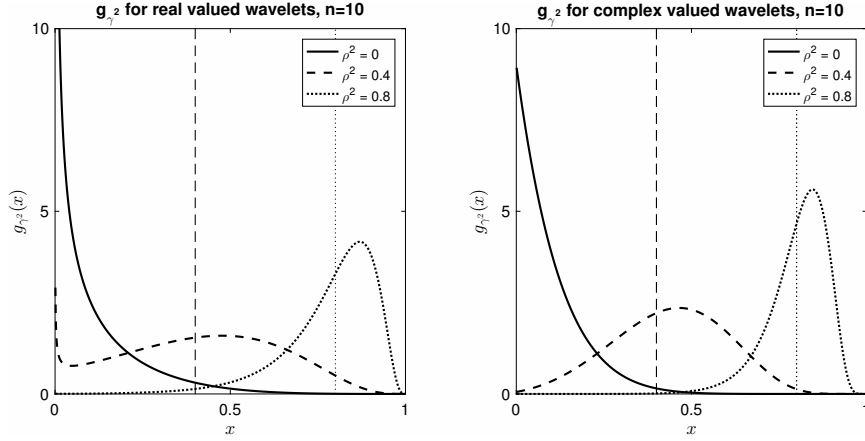


Figure 3: Asymptotic probability density functions for temporally smoothed wavelet coherence using real- and complex-valued wavelets. Degrees of freedom  $n = 10$  and true coherence  $\rho^2 = 0, 0.4$ , and  $0.8$  (marked with the vertical lines)

This distribution was first derived in Fisher (1928) for the multiple correlation coefficient and shown in Fig. 3. The proof of Corollary 1 can be found in Supplementary Material Section 1.

### 4.3 Asymptotic distributional results for complex valued wavelets

**Assumption 4.** *The analysing wavelet  $\psi(t)$  is complex-valued, continuous, has approximating support  $(-\alpha/2, \alpha/2)$  for some finite  $\alpha$ , and there exists a finite  $C$  such that  $\int |\psi(t+u) - \psi(t)| dt < C|u|$  for all real  $u$ . Furthermore, it is orthogonal to its complex conjugate, i.e.  $\int_{-\infty}^{\infty} \psi(t)\psi(t) dt = 0$ .*

The Morlet wavelet, for example, is a complex valued wavelet that satisfies Assumption 4.

In the following theorem,  $\mathcal{N}_p^C(\mu, \Sigma)$  denotes the (circular)  $p$ -dimensional complex normal distribution with mean  $\mu$  and covariance matrix  $\Sigma$ .

**Theorem 3.** *Let  $N(t)$  be a  $p$ -dimensional stationary process satisfying Assumption 1 and with spectral density matrix  $S(f)$ . Let  $\psi(t)$  be a wavelet with central frequency  $f_0$  satisfying Assumption 4. If  $a = \epsilon T/\alpha$ ,  $0 < \epsilon < 1$ , such that  $(a, b) \in \mathcal{T}_{\alpha, T}$ , then as  $T \rightarrow \infty$ , the*

continuous wavelet transform  $w(a, b)$  is asymptotically  $\mathcal{N}_p^C(0, S(f_0/a))$  for all  $b \in (a\alpha/2, T - a\alpha/2)$ .

The proof of Theorem 3 is in Supplementary Material Section 1.

Let  $\mathcal{W}_p^C(n, \Sigma)$  denote the  $p$ -dimensional complex Wishart distribution with  $n$  degrees of freedom and centrality matrix  $\Sigma$ .

**Theorem 4.** *Let  $N(t)$  be a  $p$ -dimensional stationary process satisfying Assumption 1 with spectral density matrix  $S(f)$ . Let  $h(t)$  be a smoothing window satisfying Assumption 2, let  $\psi(t)$  be a wavelet with central frequency  $f_0$  satisfying Assumption 4, and let  $\{\eta_l; l = 0, 1, \}$  be the eigenvalues of the kernel  $K(s, t)$  defined in (S4). If  $a = \epsilon T/(\alpha + \kappa)$ ,  $0 < \epsilon < 1$ , such that  $(a, b) \in \mathcal{T}_{\alpha, \kappa, T}$ , then as  $T \rightarrow \infty$ , the temporally smoothed wavelet periodogram  $\Omega(a, b)$  is asymptotically  $(1/n)\mathcal{W}_p^C(n, S(f_0/a))$  for all  $b \in (a(\alpha + \kappa)/2, T - a(\alpha + \kappa)/2)$ , where  $n = 1/(\sum_{l=1}^{\infty} \eta_l^2)$ .*

The proof of Theorem 4 is in Supplementary Material Section 1. The following distributional result for the wavelet coherence is now immediate from Theorem 4 and Goodman (1963).

**Corollary 2.** *Under the conditions of Theorem 4, the temporally smoothed wavelet coherence  $\gamma_{ij}^2(a, b) = |\Omega_{ij}(a, b)|^2/(\Omega_{ii}(a, b)\Omega_{jj}(a, b))$  between component processes  $N_i(t)$  and  $N_j(t$ ) ( $i \neq j$ ) asymptotically has density function*

$$g_{\gamma^2}(x) = (n-1)(1-\rho^2)^n(1-x)^{n-2} {}_2F_1(n, n; 1; \rho^2 x)$$

where  $\rho^2$  is shorthand for  $\rho_{ij}^2(f_0/a)$ , the spectral coherence between  $N_i(t)$  and  $N_j(t)$  at frequency  $f_0/a$ .

This density function is plotted in Fig. 3.

## 4.4 Simulations

The theoretical results presented here are verified via Monte Carlo simulations. Fig. 4 shows example QQ plots verifying both the asymptotic normality of the wavelet transform, as

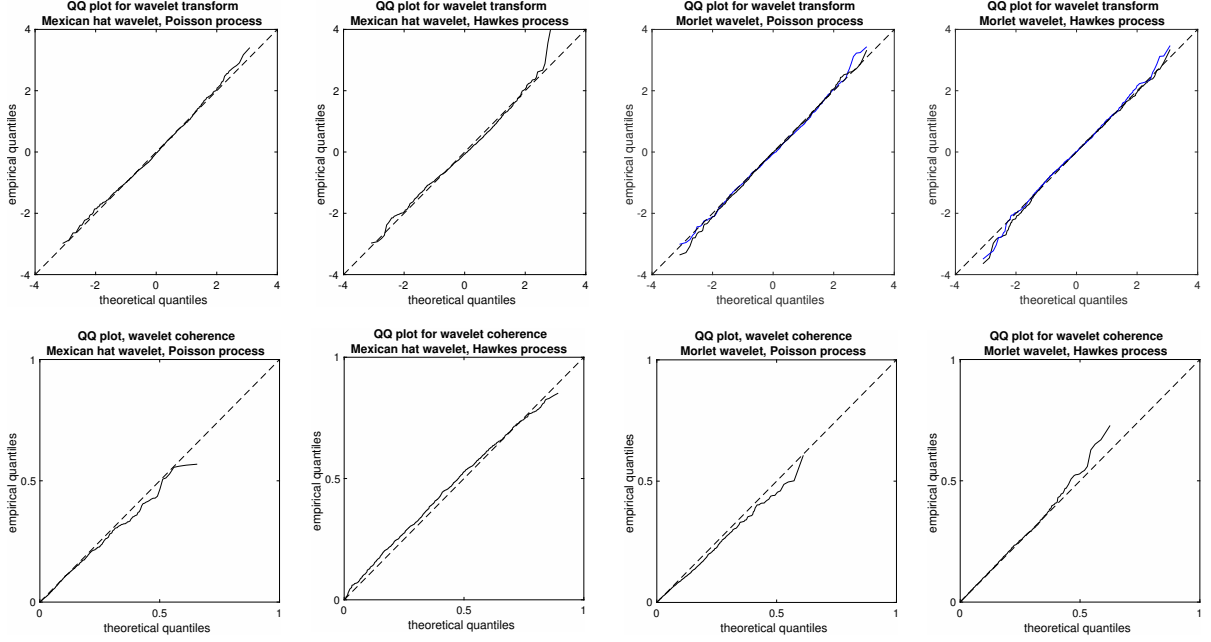


Figure 4: QQ plots verifying the presented asymptotic results for the wavelet transform and the temporally smoothed wavelet coherence using Mexican hat and Morlet wavelets.

presented in Theorems 1 and 3, and the asymptotic distribution for the wavelet coherence, as presented in Corollaries 1 and 2.

For the wavelet transform, the ordered values of  $\sigma^{-1}w(a, b)$  ( $\sigma^2 = S(f_0/a)$ ) from 1000 simulations are plotted against the theoretical quantiles of the standard normal. Two univariate processes were used. The first is a homogeneous Poisson process which has no internal correlation structure and therefore has a flat spectrum of  $S(f) = \lambda$ . The second is a Hawkes process (Hawkes, 1971) which possesses internal correlation and whose spectral density function is given in Supplementary Material Section 2 where precise details on the simulations are also provided, together with further QQ plots demonstrating the asymptotic results are robust for small  $T$ . In this example,  $T = 100$ ,  $b = 50$ , and  $a = 80/\alpha$  where  $\alpha = 10$  for the Mexican hat wavelet and  $\alpha = 8$  for the Morlet wavelet.

For the wavelet coherence QQ plots, the ordered values of  $\gamma_{12}^2(a, b)$  from 1000 simulations are plotted against the theoretical quantiles of the stated distributions. Two bivariate processes were used. The first is a pair of independent homogeneous Poisson processes. For

this process, the true spectral coherence  $\rho^2$  equals zero for all frequencies. The second is a bivariate Hawkes process (Hawkes, 1971), which contains both internal and cross correlation structure, and therefore positive coherence. Exact details of the simulations are given in Supplementary Material Section 2. In this example, again  $T = 100$ ,  $b = 50$ , and  $a = 80/(\alpha + \kappa)$  where  $\alpha = 10$  for the Mexican hat wavelet and  $\alpha = 8$  for the Morlet wavelet. A rectangular smoothing window was used with  $\kappa = 20$ , resulting in 11.57 and 8.31 degrees of freedom, respectively.

To demonstrate the ability of temporally smoothed wavelet coherence to detect non-stationary correlation structure, we compose a piecewise stationary bivariate point process. On the interval  $(0, 500]$ , the two component processes are independent Hawkes processes with zero coherence. On the interval  $(500, 1000]$  the processes switch to being mutually exciting Hawkes processes with positive coherence, and on the interval  $(1000, 1500]$  the processes revert to being independent again. Exact details are given in Supplementary Material Section 2. Fig. 5a shows the temporally smoothed wavelet coherence for a single realisation of the described process using a Morlet wavelet and smoothing parameter  $\kappa = 10$ . Fig. 5b highlights those regions of the time-scale space for which the coherence is larger than the 95th percentile of the null distribution (0.593), clearly demonstrating its ability to detect non-stationary correlation structure.

## 5 Real data example

We apply the presented methods to the analysis of signalling regions within the mouse *lateral geniculate nucleus (LGN)*. Specifically, we consider a set of neurons examined in Tang et al. (2015), where the authors are primarily concerned with analysing the firing properties of neurons in order to understand how visual signals are encoded and transferred throughout the brain. As an example, we consider only one of the experiments in the paper whereby a mouse is shown a visual stimulus in the form of an LCD screen displaying a sinusoidal monochromatic drifting grating. We here study the experiment described in Tang et al. (2015) with a spatial frequency of 0.04c/second and temporal flicker of 1Hz.

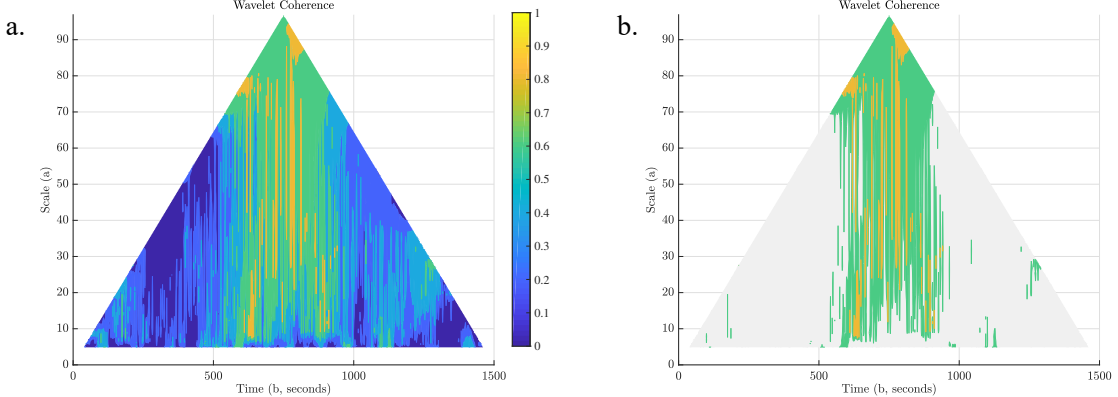


Figure 5: a. Temporally smoothed wavelet coherence estimated from a single realisation of a piecewise stationary bivariate Hawkes process. b. Temporally smoothed wavelet coherence values above the 95th percentile of the null (zero coherence) distribution.

Each trial of this data is 7 seconds in length, and as a means of illustrating the power of wavelet coherence we simply assess the coherence within a single trial of data for cell IDs 108 and 117 (these cells were picked for the example as they demonstrate relatively high firing rates). We use the Morlet wavelet with temporal smoothing parameter  $\kappa = 10$ .

The results of the experiment are provided in Fig. 6 whereby we plot the wavelet coherence derived from the smoothed spectra alongside a version showing only those values of the coherence that exceed the 95th percentile (0.593). In this case, we see what appears to be a region of coherent signalling between two cells forming in the latter half of the trial at scales between 0.2 and 0.3, corresponding to the frequency range of 3.33Hz to 5Hz. Whether such patterns are neurologically significant would require further systematic analysis. Furthermore, the question of how to combine analyses over multiple trials provides an interesting topic for future work.

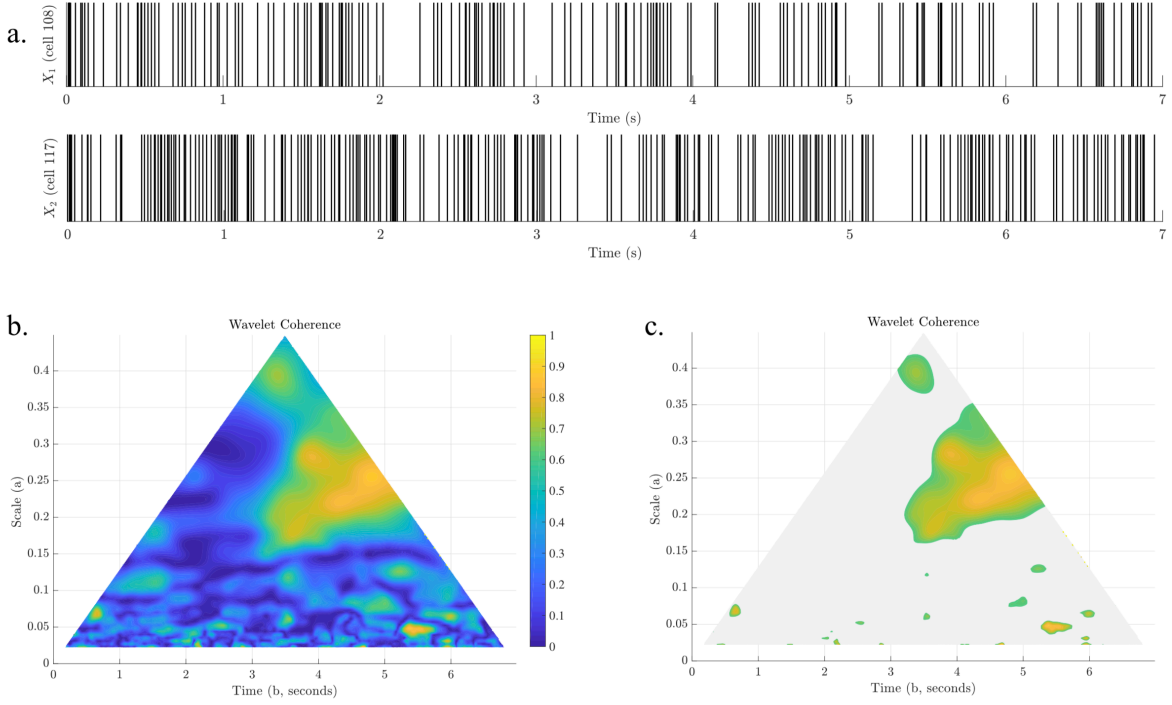


Figure 6: a. Example of neuron firing patterns for two cells in the mouse brain. b. Wavelet coherence estimated from the mouse neuron firing data. c. Temporally smoothed wavelet coherence values above the 95th percentile of the null (zero coherence) distribution.

## Acknowledgement

This work is funded by EPSRC grant EP/P011535/1. The authors would like to thank Leigh Shlomovich, Department of Mathematics, Imperial College London for developing the Hawkes process simulation code, and Heather Battey, Dean Bodenham, and Andrew Walden, Department of Mathematics, Imperial College London for stimulating conversations.

## Supplementary material

Supplementary Material Section 1 contains the proofs to propositions, theorems and corollaries presented here. Supplementary Material Section 2 provides details on the simulations contained in this paper, as well as further supporting figures. It also contains a link to a MATLAB package for implementing the presented methods.

## Appendix 1

### Computing eigen-wavelets and eigenvalues

The Nystrom method (Kythe & Puri, 2001, Chapter 1) is an efficient method for computing the eigenfunctions of kernel  $K(s, t)$  for the multiwavelet representation described in Section 3. We can approximate the integral using the quadrature rule to solve the approximate eigen-problem  $\sum_{j=1}^n w_j K(s, t_j) \tilde{\varphi}_l(t_j) = \tilde{\eta} \tilde{\varphi}_l(s)$  for a discrete set of values for  $s$ . The quadrature points  $\{t_1, \dots, t_n\}$  ( $n$  large) are regularly spaced across  $(-(\alpha + \kappa)/2, (\alpha + \kappa)/2)$  and the weights are set to be  $w_j = (\alpha + \kappa)/n$ . For simplicity, the Nystrom points  $\{s_1, \dots, s_n\}$  are set to equal  $\{t_1, \dots, t_n\}$ . In matrix form, the eigen-problem now becomes

$$KW\tilde{\varphi} = \tilde{\eta}\tilde{\varphi},$$

where  $K$  is the  $\mathbb{R}^{n \times n}$  matrix  $(K(s_i, t_j))$ ,  $\tilde{\varphi} \equiv [\tilde{\varphi}(t_1), \dots, \tilde{\varphi}(t_n)]^T$ , and  $W \equiv \text{diag}(w_1, \dots, w_n)$ . Solving the above gives approximations to the first  $n$  eigenvalues and eigen-wavelets of kernel  $K(s, t)$ .

Should it be required, the Nystrom extension of the sampled vector  $\tilde{\varphi}_l = [\tilde{\varphi}(s_1), \dots, \tilde{\varphi}(s_n)]$  is the function

$$\tilde{\varphi}_l(x) = \tilde{\lambda}_l \sum_{j=1}^n w_j K(x, s_j) \tilde{\varphi}_l(s_j).$$

The sum in (S5) is over an infinite set of (eigen-)wavelet periodograms. However, in practice, the size of the eigenvalues drop away rapidly indicating that the kernel can be ac-

curately reconstructed using only small number of its eigen-wavelets, hence (S5) can be approximated with only a small number of terms. For example, in the case of the  $\kappa = 10$ , the first nine eigenvalues contain 99.9% (3.s.f.) of the overall energy.

## References

- BARTLETT, M. S. (1963). The Spectral Analysis of Point Processes. *Journal of the Royal Statistical Society. Series B* **25**, 264–296.
- BRILLINGER, D. R. (1972). The spectral analysis of stationary interval functions. *Proceedings of the Sixth Berkeley Symposium on Mathematical Statistics and Probability, Volume 1: Theory of Statistics* , 483–513.
- BRILLINGER, D. R. (1996). Some uses of cumulants in wavelet analysis. *Journal of Nonparametric Statistics* **6**, 93–114.
- CARTER, G. (1987). Coherence and time delay estimation. *Proceedings of the IEEE* **75**, 236–255.
- COHEN, E. A. K. & WALDEN, A. T. (2010a). A statistical analysis of Morse wavelet coherence. *IEEE Transactions on Signal Processing* **58**, 980–989.
- COHEN, E. A. K. & WALDEN, A. T. (2010b). A Statistical Study of Temporally Smoothed Wavelet Coherence. *IEEE Transactions on Signal Processing* **58**, 2964–2973.
- FISHER, R. A. (1928). The general sampling distribution of the multiple correlation coefficient. *Proceedings of the Royal Society Series A* **121**.
- GOODMAN, N. (1963). Statistical Analysis Based on a Certain Multivariate Complex Gaussian Distribution (An Introduction). *Annals of Mathematical Statistics* **34**, 152–177.
- HAWKES, A. G. (1971). Spectra of Some Self-Exciting and Mutually Exciting Point Processes. *Biometrika* **58**, 83–90.

KYTHE, P. K. & PURI, P. (2001). *Computational Methods for Linear Integral Equations*. Springer.

MERCER, J. (1909). Functions of Positive and Negative Type, and their Connection with the Theory of Integral Equations. *Philosophical Transactions of the Royal Society A: Mathematical, Physical and Engineering Sciences* **209**, 415–446.

OLHEDE, S. C. & WALDEN, A. T. (2002). Generalized Morse wavelets. *IEEE Transactions on Signal Processing* **50**, 2661–2670.

TANG, S., ARDILA JIMENEZ, S. C., CHAKRABORTY, S. & SCHULTZ, S. R. (2015). Visual receptive field properties of neurons in the mouse lateral geniculate nucleus. *Plos One* **11**, 1–34.

THOMSON, D. J. (1982). Spectrum Estimation and Harmonic Analysis. *Proceedings of the IEEE* **70**.

WALDEN, A. T. (2000). A unified view of multitaper multivariate spectral estimation. *Biometrika* **87**, 767–788.

WELCH, P. (1967). The use of fast fourier transform for the estimation of power spectra: a method based on time averaging over short, modified periodograms. *IEEE Transactions on Audio Electroacoustics* **15**, 70–73.

## Correspondence

Correspondence should be addressed to

Edward Cohen  
Department of Mathematics  
Imperial College London  
London SW7 2AZ.

Email: e.cohen@imperial.ac.uk

# Supplementary Material

## Wavelet Spectra for Multivariate Point Processes

E.A.K. Cohen and A.J. Gibberd

## 1 Proofs

Where relevant,  $a$  and  $b$  are such that  $(a, b) \in \mathcal{T}_{\alpha, T}$  or  $(a, b) \in \mathcal{T}_{\alpha, \kappa, T}$ . This allows all integrals over  $(0, T)$  to be replaced by integrals over the entire real line.

While in the main manuscript it makes sense to present Proposition 1 before Proposition 2, for the purposes of proving these results, it makes sense to prove Proposition 2 first.

### Proof of Proposition 2

*Proof.* Let  $\mathcal{F}\{\cdot\}$  denote the Fourier transform. From the convolution theorem it holds that

$$\begin{aligned} \sum_{l=0}^{\infty} \eta_l |\Phi_l(f)|^2 &= \sum_{l=0}^{\infty} \eta_l \mathcal{F}\{\varphi_l * \varphi_l^*\}(f) \\ &= \sum_{l=0}^{\infty} \eta_l \int \left( \int \varphi_l(\tau) \varphi_l^*(t - \tau) d\tau \right) e^{-i2\pi f t} dt. \end{aligned}$$

With  $K(s, t) = \sum_{l=0}^{\infty} \eta_l \varphi_l(s) \varphi_l^*(t)$ , it follows that

$$\begin{aligned} \sum_{l=0}^{\infty} \eta_l |\Phi_l(f)|^2 &\equiv \mathcal{F} \left\{ \int K(\tau, t - \tau) d\tau \right\} (f) \\ &= \mathcal{F} \left\{ \int \int h(b') \psi(\tau - b') \psi^*(t - \tau - b') db' d\tau \right\} (f) \\ &= |\Psi(f)|^2 \int h(b') db' = |\Psi(f)|^2. \end{aligned}$$

□

We can now easily proceed with the proof of Proposition 1.

## Proof of Proposition 1

*Proof.* Property (i): from the definition of  $K(s, t)$  in (4), it immediately follows that  $\int \int K(s, t) ds dt = 0$ . Furthermore, with  $K(s, t) = \sum_{l=0}^{\infty} \eta_l \varphi_l(s) \varphi_l^*(t)$ , it follows that

$$\int \int K(s, t) ds dt = \sum_{l=0}^{\infty} \left| \int \varphi_l(t) dt \right|^2.$$

Therefore  $\left| \int \varphi_l(t) dt \right| = 0$  for all  $\varphi_l(t)$  with positive eigenvalues.

Property (ii) is immediate from the construction of the eigenfunctions.

Property (iii) is immediate from Proposition 1 and the fact that  $\psi(t)$  itself obeys the admissibility condition.  $\square$

## Proof of Proposition 3

*Proof.* From (5), it follows that  $E(\Omega(a, b)) = \sum_{l=0}^{\infty} \eta_l E(v_l(a, b) v_l^H(a, b))$ . With  $v_l(a, b) = \int \varphi_l((t - b)/a) dN(t)$ , it follows that

$$\begin{aligned} E(v_l(a, b) v_l^H(a, b)) &= \int \int \varphi_l((t - b)/a) \varphi_l((s - b)/a) \Gamma(t, s) dt ds \\ &= \int \int \varphi_l((t - b)/a) \varphi_l((t - \tau - b)/a) \Gamma(\tau) dt d\tau \\ &= \int |\Phi_l(af)|^2 S(f) df. \end{aligned}$$

Therefore, from Proposition 2

$$E(\Omega(a, b)) = E(W(a, b)) = \int_{-\infty}^{\infty} |\Psi(af)|^2 S(f) df.$$

Taking the Taylor expansion of  $S(f)$  around  $f_a = f/a$  gives

$$\begin{aligned} \int_{-\infty}^{\infty} |\Psi(af)|^2 S(f) df &= \int_{-\infty}^{\infty} |\Psi(af)|^2 (S(f_a) + (f - f_a) S'(f_a) + \frac{(f - f_a)^2}{2!} S''(f_a) + \dots) df \\ &= S(f_a) + S''(f_a) \int_{-\infty}^{\infty} |\Psi(af)|^2 \frac{(f - f_a)^2}{2!} df + \dots \\ &= S(f_a) + O(\tilde{\epsilon}^{-2} T^{-2}) \end{aligned}$$

from the Fourier transform uncertainty principle and noting  $a = \tilde{\epsilon}T$ .  $\square$

## Lemmas for Theorems 1-4 and Corollary 1

The following Lemma is presented as Corollary 3.1 in Brillinger (1972).

**Lemma 1.** *Let  $N(t)$  be a  $p$ -dimensional point process satisfying Assumption 1, and let  $\xi_1(t), \dots, \xi_k(t)$  be a continuous functions with finite support, then*

$$\begin{aligned} \text{cum} \left\{ \int \xi_1(t_1) dN_{i_1}(t_1), \dots, \int \xi_k(t_k) dN_{i_k}(t_k) \right\} &= \sum_{l=1}^k \sum_{\alpha_1, \dots, \alpha_l=1}^p \left[ \prod_{j \in v_1} \delta_{\alpha_1 i_j} \right] \dots \left[ \prod_{j \in v_l} \delta_{\alpha_l i_j} \right] \\ &\times \int \dots \int \left( \prod_{j \in v_1} \xi_j(\tau_1) \right) \dots \left( \prod_{j \in v_l} \xi_j(\tau_l) \right) q_{\alpha_1, \dots, \alpha_l}(\tau_1, \dots, \tau_l) d\tau_1, \dots, d\tau_l, \quad (\text{S1}) \end{aligned}$$

where  $\delta_{ij} = 1$  if  $i = j$  and is zero otherwise.

The first summation in (S1) does not have just  $k$  terms, but instead extends over all partitions of  $\{1, \dots, k\}$  of the form  $(v_1, \dots, v_l)$ . For example, for  $k = 3$ , the  $l = 1$  partition is  $(\{1, 2, 3\})$ , the  $l = 2$  partitions are  $(\{1\}, \{2, 3\})$ ,  $(\{2\}, \{1, 3\})$  and  $(\{3\}, \{1, 2\})$ , and the  $l = 3$  partition is  $(\{1\}, \{2\}, \{3\})$ , resulting in 5 terms. To proceed, we will also require the following lemma.

**Lemma 2.** *Let  $N(t)$  be a point process satisfying Assumption 1, and let  $\psi_1(t)$  and  $\psi_2(t)$  be a pair of orthogonal wavelets, each satisfying either Assumption 3 (real-valued wavelets) or Assumption 4 (complex-valued wavelets). The cumulant*

$$\text{cum} \left\{ T^{-1/2} \int \psi_1(t_1/T) dN_{i_1}(t_1), T^{-1/2} \int \psi_2^*(t_2/T) dN_{i_2}(t_2) \right\}$$

is  $O(T^{-1})$ .

*Proof.* From Lemma 1, the cumulant equals

$$T^{-1} \int \int \psi_1 \left( \frac{t+u}{T} \right) \psi_2^* \left( \frac{t}{T} \right) r_{i_1, i_2}(u) du dt.$$

The stated orthogonality of  $\psi_1(t)$  and  $\psi_2(t)$  implies  $\int \psi_1(t)\psi_2^*(t)dt = 0$ . It follows from Assumption 3 (real-valued) or Assumption 4 (complex-valued) that

$$\begin{aligned}
& \left| T^{-1} \int \int \psi_1 \left( \frac{t+u}{T} \right) \psi_2^* \left( \frac{t}{T} \right) r_{i_1, i_2}(u) du dt \right| \\
&= \left| T^{-1} \int \int \psi_1 \left( \frac{t+u}{T} \right) \psi_2^* \left( \frac{t}{T} \right) r_{i_1, i_2}(u) du dt - T^{-1} \int \int \psi_1 \left( \frac{t}{T} \right) \psi_2^* \left( \frac{t}{T} \right) r_{i_1, i_2}(u) du dt \right| \\
&\leq T^{-1} \int \int \left| \psi_1 \left( \frac{t+u}{T} \right) \psi_2^* \left( \frac{t}{T} \right) - \psi_1 \left( \frac{t}{T} \right) \psi_2^* \left( \frac{t}{T} \right) \right| |r_{i_1, i_2}(u)| dt du \\
&\leq T^{-1} C' \int |u| |r_{i_1, i_2}(u)| du,
\end{aligned}$$

for some finite  $C'$ . The required result follows from Assumption 1.  $\square$

**Lemma 3.** *Let  $\psi(t)$  be a complex valued wavelet satisfying Assumption 4, and  $h(t)$  a real valued, compactly supported smoothing window that generate kernel  $K(s, t)$ . The eigenwavelets of  $K(s, t)$  also satisfy Assumption 4.*

*Proof.* The variability condition follows trivially from variability condition on  $\psi(t)$ . The orthogonality condition follows from the orthogonality condition on  $\psi(t)$ . Specifically, it is true that  $\int \int K(s, t)K(s, t)ds dt = 0$ . Furthermore,

$$\int \int K(s, t)K(s, t)ds dt = \sum_{l=0}^{\infty} \eta_l^2 \left( \int \varphi_l(t)\varphi_l(t)dt \right)^2.$$

Therefore  $\int \varphi_l(t)\varphi_l(t)dt = 0$  for  $l = 0, 1, \dots$ .  $\square$

## Proof of Theorem 1

*Proof.* We first verify the mean and covariance of  $w(a, b)$  are as given. The mean is  $E(w(a, b)) = E(\int_0^T \psi^*((t-b)/a)dN(t)) = \int_0^T \psi^*((t-b)/a)E(dN(t)) = \int_0^T \psi^*((t-b)/a)\lambda(t)dt$ . Under the assumptions of the theorem,  $N(t)$  is stationary, hence  $\lambda(t)$  is constant for all  $t$  and  $E(w(a, b)) = 0$  as the wavelet integrates to zero. The asymptotic result for  $\text{cov}(w(a, b)) = E(W(a, b))$  is given in Proposition 3. The first and second order cumulants are therefore asymptotically equal to those stated in the theorem.

To conclude, we are required to show that all cumulants of order greater than two asymptotically go to zero. From Lemma 1,

$$\begin{aligned} \text{cum}\{w_{i_1}(a, b), \dots, w_{i_k}(a, b)\} &= \sum_{l=1}^k \sum_{\alpha_1, \dots, \alpha_l=1}^p \left[ \prod_{j \in v_1} \delta(\alpha_1 - a_j) \right] \dots \left[ \prod_{j \in v_l} \delta(\alpha_l - a_j) \right] \\ &\times \int \dots \int \psi_{a,b}^{|v_1|}(\tau_1) \dots \psi_{a,b}^{|v_l|}(\tau_l) q_{\alpha_1, \dots, \alpha_l}(\tau_1, \dots, \tau_l) d\tau_1, \dots, d\tau_l. \end{aligned} \quad (\text{S2})$$

Through a change of variables, under Assumption 1, it follows that

$$\begin{aligned} \text{cum}\{w_{i_1}(a, b), \dots, w_{i_k}(a, b)\} &= T^{-k/2} \sum_{l=1}^k \sum_{\alpha_1, \dots, \alpha_l=1}^p \left[ \prod_{j \in v_1} \delta(\alpha_1 - a_j) \right] \dots \left[ \prod_{j \in v_l} \delta(\alpha_l - a_j) \right] \\ &\int \dots \int \psi_{\tilde{\epsilon}}^{|v_1|} \left( \frac{t+u_1}{T} \right) \dots \psi_{\tilde{\epsilon}}^{|v_{l-1}|} \left( \frac{t+u_{l-1}}{T} \right) \psi_{\tilde{\epsilon}}^{|v_l|} \left( \frac{t}{T} \right) r_{\alpha_1, \dots, \alpha_l}(u_1, \dots, u_{l-1}) du_1, \dots, du_{l-1} dt, \end{aligned} \quad (\text{S3})$$

where for  $\tilde{\epsilon} = \epsilon/\alpha$ ,  $\psi_{\tilde{\epsilon}}(t) = \tilde{\epsilon}^{-1/2} \psi(t/\tilde{\epsilon})$ . Recognising that the product of Kronecker deltas is either zero or one gives

$$\begin{aligned} |\text{cum}\{w_{i_1}(a, b), \dots, w_{i_k}(a, b)\}| &\leq T^{-k/2} \sum_{l=1}^k \sum_{\alpha_1, \dots, \alpha_l=1}^p \\ &\int \dots \int \left| \psi_{\tilde{\epsilon}}^{|v_1|} \left( \frac{t+u_1}{T} \right) \dots \psi_{\tilde{\epsilon}}^{|v_{l-1}|} \left( \frac{t+u_{l-1}}{T} \right) \psi_{\tilde{\epsilon}}^{|v_l|} \left( \frac{t}{T} \right) r_{\alpha_1, \dots, \alpha_l}(u_1, \dots, u_{l-1}) \right| du_1 \dots du_{l-1} dt. \end{aligned} \quad (\text{S4})$$

Using the fact that  $\sum_{j=1}^l |v_j| = k$ , Hölder's inequality gives

$$\begin{aligned} &\int \left| \psi_{\tilde{\epsilon}}^{|v_1|} \left( \frac{t+u_1}{T} \right) \dots \psi_{\tilde{\epsilon}}^{|v_{l-1}|} \left( \frac{t+u_{l-1}}{T} \right) \psi_{\tilde{\epsilon}}^{|v_l|} \left( \frac{t}{T} \right) \right| dt \\ &\leq \prod_{\beta=1}^{l-1} \left( \int \left| \psi_{\tilde{\epsilon}} \left( \frac{t+u_l}{T} \right) \right|^k dt \right)^{|v_\beta|/k} \left( \int \left| \psi_{\tilde{\epsilon}} \left( \frac{t}{T} \right) \right|^k dt \right)^{|v_l|/k} \\ &= \int \left| \psi_{\tilde{\epsilon}} \left( \frac{t}{T} \right) \right|^k dt = \tilde{\epsilon}^{1-k/2} A_k T \end{aligned} \quad (\text{S5})$$

where  $A_k = \int |\psi(t)|^k dt$ . Putting (S4) and (S5) together, it follows that

$$\begin{aligned} &|\text{cum}\{w_{i_1}(a, b), \dots, w_{i_k}(a, b)\}| \\ &\leq (\tilde{\epsilon} T)^{1-k/2} A_k \sum_{l=1}^k \sum_{\alpha_1, \dots, \alpha_l=1}^p \int \dots \int |r_{\alpha_1, \dots, \alpha_l}(u_1, \dots, u_{l-1})| du_1, \dots, du_{l-1}. \end{aligned} \quad (\text{S6})$$

Therefore, from Assumption 1,  $\text{cum}\{w_{i_1}(a, b), \dots, w_{i_k}(a, b)\}$  is  $O(\tilde{\epsilon}^{1-k/2} T^{1-k/2})$  and tends to zero as  $T \rightarrow \infty$  for all  $k > 2$ .  $\square$

## Proof of Theorem 2

*Proof.* Consider the eigenwavelet representation of the TSWP in (9). According to Theorem 1,  $v_i(a, b)$  is asymptotically  $\mathcal{N}(0, S(f_0/a))$ ,  $i = 0, 1, \dots$ . Therefore  $v_i(a, b)v_i(a, b)^T$  is asymptotically  $\mathcal{W}_p(1, S(f_0/a))$ . As the eigenwavelet system is orthonormal, Lemma 2 states that  $v_0(a, b), v_1(a, b), \dots$  are asymptotically independent random vectors and therefore it follows in an analogous manner to (Walden, 2000, p. 776) that  $\Omega(a, b)$  is asymptotically  $(1/n)\mathcal{W}_p(n, S(f_0/a))$  where  $n = 1/\sum_{k=0}^{\infty} \eta_i^2$ .  $\square$

## Proof of Corollary 1

*Proof.* Let  $\Omega^{ij}(a, b)$  be the  $\mathbb{R}^{2 \times 2}$  matrix made up of the  $i$ th and  $j$ th columns and rows of  $\Omega(a, b)$ . It is immediate from Theorem 2 that asymptotically  $\Omega^{ij} \sim \mathcal{W}_2(n, S(f_0/a))$  and from Theorem 5.3.2 of Muirhead (1985) (first presented in Fisher (1928)) that  $\gamma_{ij}^2(a, b)$  is of the stated distribution.  $\square$

## Proof of Theorem 3

*Proof.* This proof is almost identical to the proof for Theorem 1, although additionally we are required to show  $\text{cov}(w(a, b), w^H(a, b))$  is asymptotically zero for a circular complex normal distribution. We note for a pair of complex random variables  $W$  and  $Z$ ,  $\text{cov}(W, Z^*) = \text{cum}\{W, Z\}$ . Under the theorem,  $a = \epsilon T/\alpha$  for some  $0 < \epsilon < 1$ , and hence

$$\begin{aligned} \text{cov}(w_{i_1}(a, b), w_{i_2}^*(a, b)) &= \text{cum} \left\{ a^{-1/2} \int \psi \left( \frac{t_1 - b}{a} \right) dN_{i_1}(t_1), a^{-1/2} \int \psi \left( \frac{t_2 - b}{a} \right) dN_{i_2}(t_2) \right\} \\ &= \text{cum} \left\{ T^{-1/2} \int \psi_{\tilde{\epsilon}} \left( \frac{t_1 - b}{T} \right) dN_{i_1}(t_1), T^{-1/2} \int \psi_{\tilde{\epsilon}} \left( \frac{t_2 - b}{T} \right) dN_{i_2}(t_2) \right\}, \end{aligned}$$

where for  $\tilde{\epsilon} = \epsilon/\alpha$ ,  $\psi_{\tilde{\epsilon}}(t) = \tilde{\epsilon}^{-1/2}\psi(t/\tilde{\epsilon})$ . Assumption 4 implies  $\psi_{\tilde{\epsilon}}(t)$  is orthogonal to  $\psi_{\tilde{\epsilon}}^*(t)$ . Setting  $\psi_1(t) = \psi_{\tilde{\epsilon}}(t)$  and  $\psi_2(t) = \psi_{\tilde{\epsilon}}^*(t)$  in Lemma 2 gives  $\text{cov}(w(a, b), w^H(a, b))$  as  $O(\tilde{\epsilon}^{-1}T^{-1})$ . The first and second order cumulants are therefore asymptotically equal to those stated in the theorem.

The proof that all cumulants of order greater than two asymptotically go to zero is identical to that given in the proof to Theorem 1, which trivially extends to cumulants that include complex conjugates of the form  $\text{cum}\{w_{i_1}(a, b), \dots, w_{i_{k'}}(a, b), w_{i_{k'+1}}^*(a, b), \dots, w_{i_k}^*(a, b)\}$  where  $0 \leq k' \leq k$ .  $\square$

## Proof of Theorem 4

*Proof.* Consider the eigenwavelet representation of the TSWP in (9). According to Theorem 3, and additionally in the case of a complex wavelet Lemma 3,  $v_i(a, b)$  is asymptotically  $\mathcal{N}^C(0, S(f_0/a))$ ,  $i = 0, 1, \dots$ . Therefore  $v_i(a, b)v_i(a, b)^H$  is asymptotically  $\mathcal{W}_p^C(1, S(f_0/a))$ . As the eigenwavelet system is orthonormal, Lemma 2 states that  $v_0(a, b), v_1(a, b), \dots$  are asymptotically independent random vectors and therefore it follows from (Walden, 2000, p. 776) that  $\Omega(a, b)$  is asymptotically  $(1/n)\mathcal{W}_p^C(n, S(f_0/a))$  where  $n = 1/\sum_{k=0}^{\infty} \eta_i^2$ .  $\square$

## 2 Simulation details

To validate the distributional results for the wavelet transform in Theorems 1 and 3, two univariate processes were used. The first is a homogeneous Poisson process for which  $\Gamma(\tau) = \lambda\delta(\tau)$  and  $S(f) = \lambda$ . The second is a Hawkes process (Hawkes, 1971) with exponential decay. This self-exciting process contains internal correlation structure and has a stochastic intensity function of

$$\Lambda(t) = \nu + \int_{-\infty}^t \alpha \exp(-\beta(t-s))dN(s),$$

and a spectral density function

$$S(f) = \frac{\nu\beta}{\beta - \alpha} \left( 1 + \frac{\alpha(2\beta - \alpha)}{(\beta - \alpha)^2 + (2\pi f)^2} \right).$$

The Hawkes process used in the simulations has a base-intensity  $\nu = 1$ , excitation intensity  $\alpha = 0.5$ , and decay parameter  $\beta = 1$ . Both the real valued Mexican hat wavelet and the complex valued Morlet wavelet are considered at scale  $a$  that grows with  $T$  ( $\epsilon = 1/2$ ) for  $T = 10, 50$  and  $100$ . The asymptotic normality of the wavelet transform, as presented in Theorems 1 and 3, are confirmed via QQ plots in Figure 1. Here, the ordered values of  $\sigma^{-1}w(a, b)$  ( $\sigma^2 = S(f_0/a)$ ) are plotted against the theoretical quantiles of the standard normal.

To validate the distributional results of the temporally smoothed wavelet coherence in Corollaries 1 and 2, two bivariate processes were used. The first is a pair of independent homogeneous Poisson processes. It's spectral density matrix is

$$S(f) = \begin{pmatrix} \lambda & 0 \\ 0 & \lambda \end{pmatrix}$$

and has a true spectral coherence of  $\rho^2(f) = 0$ .

The second is a bivariate mutually exciting Hawkes process. This contains both inter and cross dependencies and is defined through its stochastic intensity function

$$\Lambda(t) = \nu + \int_{-\infty}^t G(t-s)dN(s),$$

where  $\nu$  is the base intensity vector and

$$G(s) = \begin{pmatrix} \alpha_{11} \exp(-\beta_{11}s) & \alpha_{12} \exp(-\beta_{12}s) \\ \alpha_{21} \exp(-\beta_{21}s) & \alpha_{22} \exp(-\beta_{22}s) \end{pmatrix}.$$

The diagonal elements of  $G(s)$  characterise the self-exciting behaviour of each individual process, and the off-diagonal elements characterise the mutually exciting behaviour. The particular process used in the simulations has  $\nu = (1, 1)^T$ ,  $\beta_{ij} = 1$  ( $i, j = 1, 2$ ),  $\alpha_{11} = \alpha_{22} = 0.5$ , and  $\alpha_{12} = \alpha_{21} = 0.4$ .

The form of the spectral matrix in this setting is non-trivial and given in Hawkes (1971). The true spectral coherence can be computed from this matrix and is shown in Figure 2.

The asymptotic distribution for the temporally smoothed wavelet coherence, as presented in Corollaries 1 and 2, are confirmed via QQ plots in Figure 3 for both the Poisson and

Hawkes processes. Here, the ordered values of  $\gamma_{12}^2(a, b)$  are plotted against the theoretical quantiles of the stated distributions. Both the real valued Mexican hat wavelet and the complex valued Morlet wavelet are considered at scale  $a$  that grows with  $T$  ( $\epsilon = 4/5$ ) for  $T = 10, 50$  and  $100$ . Translation  $b$  is set at  $T/2$  and a smoothing parameter of  $\kappa = 20$  is used, resulting in  $11.57$  degrees of freedom for the Mexican hat wavelet and  $8.31$  degrees of freedom for the Morlet wavelet.

The bivariate piecewise stationary Hawkes process used in Section 4.4 is made up of three components. On the intervals  $(0, 500]$  and  $(1000, 1500]$  are a pair independent Hawkes processes each with parameters  $\nu = (0.5, 0.5)^T$ ,  $\alpha = 0.7$  and  $\beta = 1$ . On  $(500, 1000]$  is a bivariate mutually exciting Hawkes process with  $\nu = (0.5, 0.5)^T$ ,  $\beta_{ij} = 1$  ( $i, j = 1, 2$ ),  $\alpha_{11} = \alpha_{22} = 0.2$ , and  $\alpha_{12} = \alpha_{21} = 0.5$ .

### 3 Code

Code and data associated with this paper can be found in the github repository  
<https://github.com/AlexGibberd/pointWav>.

### References

- BRILLINGER, D. R. (1972). The spectral analysis of stationary interval functions. *Proceedings of the Sixth Berkeley Symposium on Mathematical Statistics and Probability, Volume 1: Theory of Statistics* , 483–513.
- FISHER, R. A. (1928). The general sampling distribution of the multiple correlation coefficient. *Proceedings of the Royal Society Series A* **121**.
- HAWKES, A. G. (1971). Spectra of Some Self-Exciting and Mutually Exciting Point Processes. *Biometrika* **58**, 83–90.
- MUIRHEAD, R. J. (1985). *Aspects of Multivariate Statistical Theory*. John Wiley & Sons, Inc, 2nd ed.

WALDEN, A. T. (2000). A unified view of multitaper multivariate spectral estimation.  
*Biometrika* **87**, 767–788.

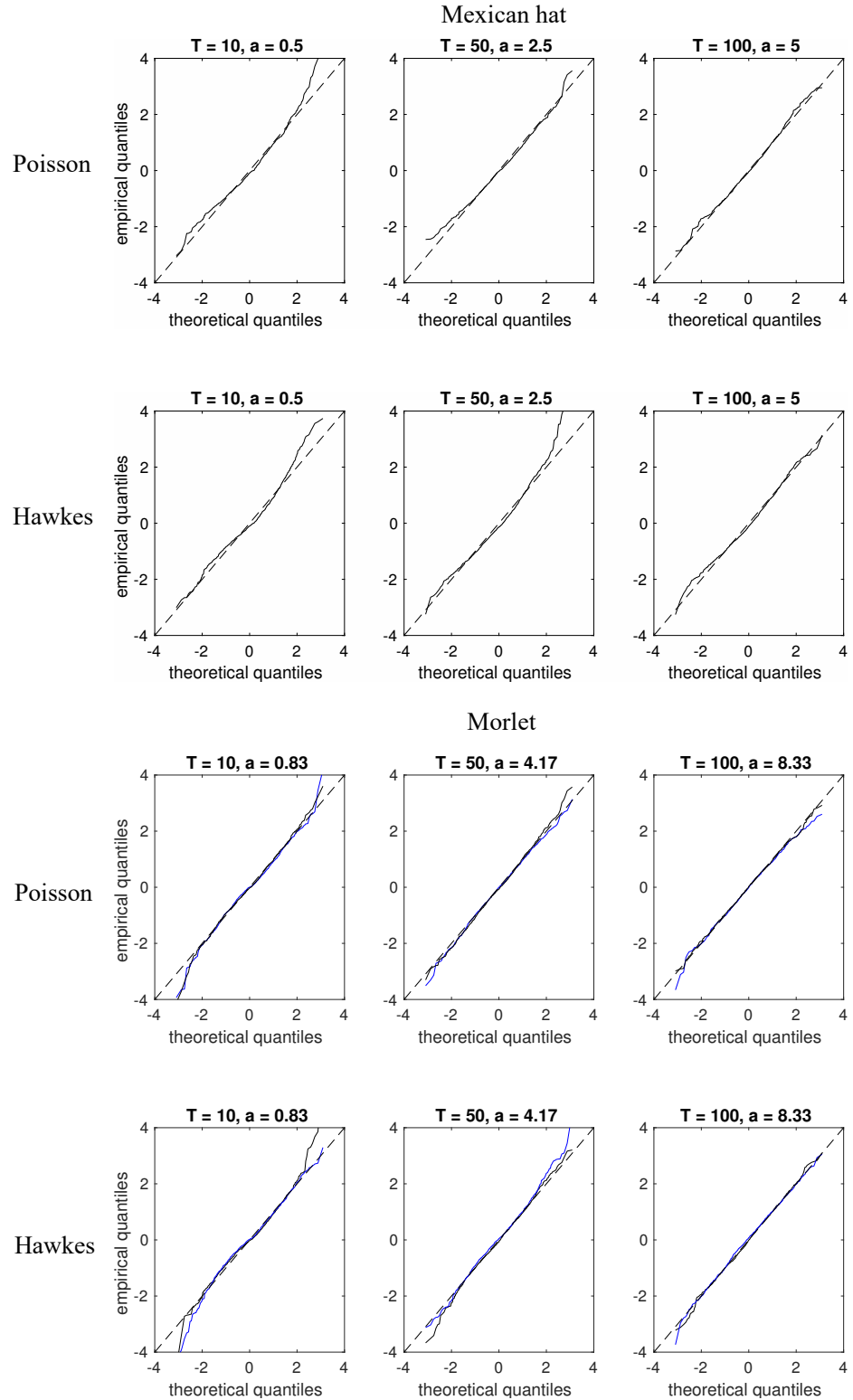


Figure 1: QQ plots for empirical quantiles of the wavelet transform against the theoretical quantiles of the normal distribution. See text for details.

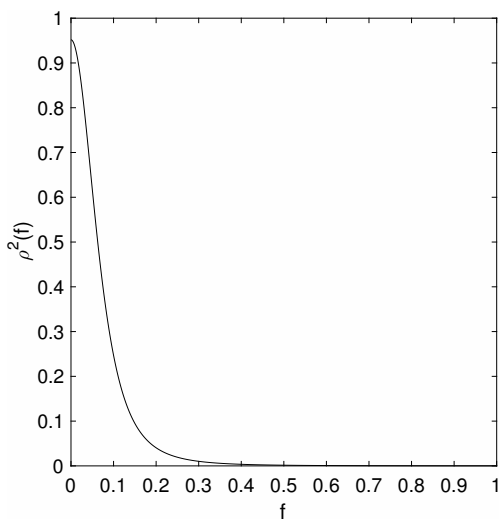


Figure 2: Spectral coherence  $\rho^2(f)$  for the bivariate mutually exciting Hawkes process described in the text.

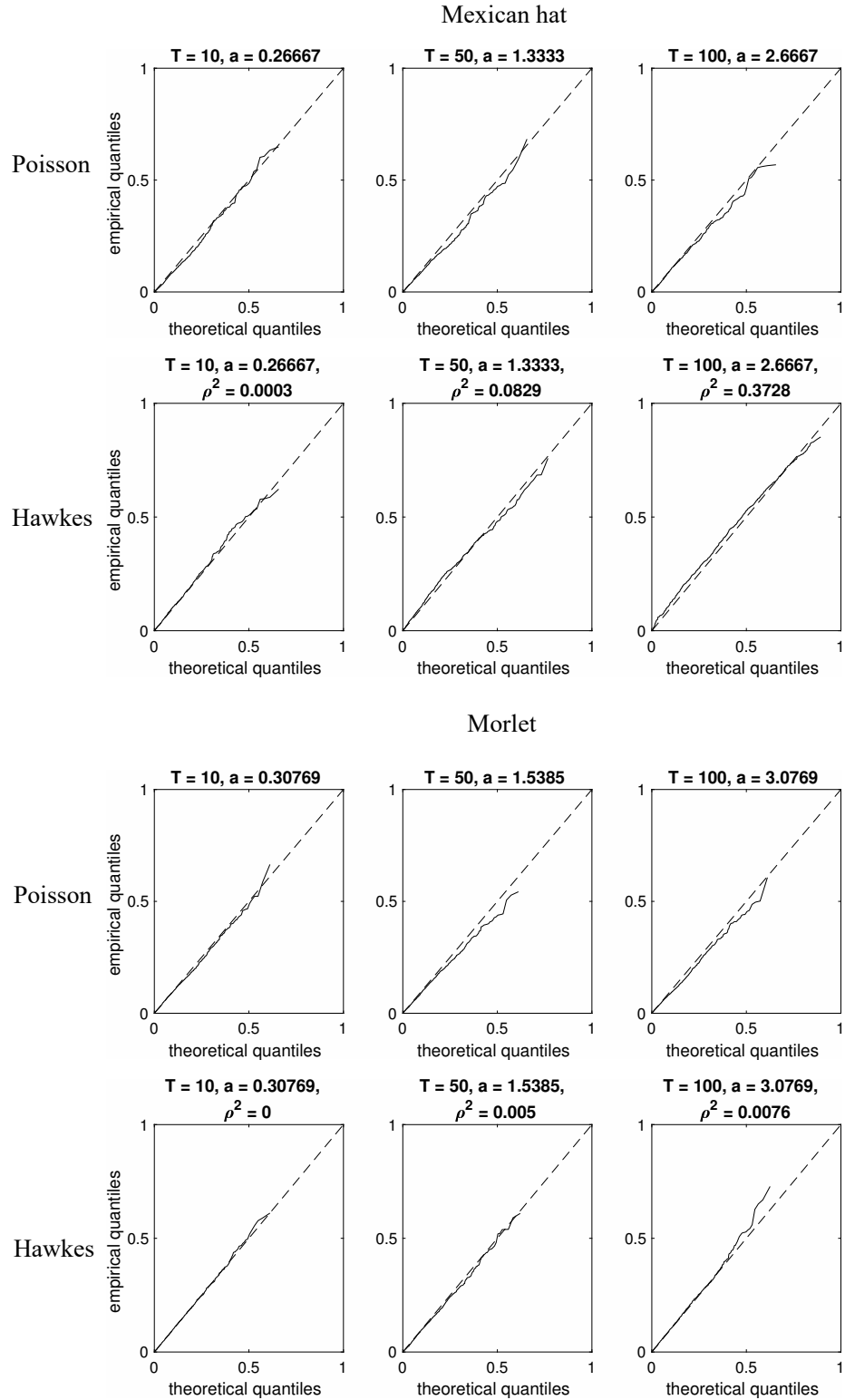


Figure 3: QQ plots for empirical quantiles of the temporally smoothed wavelet coherences against the theoretical quantiles of the asymptotic distribution. See text for details.